Electronic Annex

Surficial weathering of iron sulfide mine tailings under semi-arid climate

Sarah M. Hayes, Robert A. Root, Nicolas Perdrial, Raina Maier, and Jon Chorover*

Department of Soil, Water and Environmental Science,

University of Arizona, Tucson, AZ 85721

Submitted to:

Geochimica et Cosmochimica Acta

* Address correspondence to Jon Chorover, Department of Soil, Water and Environmental Science, University of Arizona, 1177 E 4th St, Shantz 429, Tucson, AZ 85721
Telephone: +1 520-626-5635, Fax: 520-626-1647, E-mail: chorover@cals.arizona.edu

Pages: 14

Sequential Extraction Procedure

The SSE procedure was modified after Dold (2003) and Neaman et al. (2004) and performed as follows:1) deionized water (H_2O), 1 h at room temperature (25^oC, RT), targeting soluble efflorescent salts, e.g. gypsum; 2) 1 M ammonium nitrate, 2h at RT with a DI wash targeting easily exchangeable and plant/bioavailable ions and metals; 3) 1M ammonium acetate with pH adjusted to 4.5 with acetic acid and a DI wash, targeting non-specifically sorbed ions and acid soluble carbonates; 4) 1.0M sodium phosphate (NaH_2PO_4), 24 hr with pH adjusted to 5.0 with acetic acid and a DI wash, targeting specifically sorbed ligands, e.g. inner sphere As complexed on ferric (hyr)oxide surface sites; 5) 0.1 M ascorbic acid plus 0.2 M ammonium oxalate, 2 h in the dark at pH 3.0 adjusted with oxalic acid with an acetic acid wash to dissolve precipitated oxalates , targeting poorly crystalline Al, Mn, and Fe (oxyhydr)oxides, including ferrihydrite and schwertmannite; and 6) 1 M citrate-bicarbonate-dithionite with an acetic acid wash, targeting reducible crystalline Al, Mn, and Fe (oxyhydr)oxides and (hydroxy)sulfates, including goethite and jarosite. Sediment aliquots were sequentially treated with each extractant solution (solid: solution = 1:40 by mass), the suspensions were centrifuged (25 min at 11 000 g), and the supernatant was decanted and filtered (0.45 μm nylon membrane filters). Between extraction steps, sediments were washed with 10 mL of deionized water (18.2 MΩ-cm), centrifuged, and the supernatant decanted. The filtrate from each extraction step was analyzed by ICP-MS. After these extractions were performed, the residual solids underwent elemental analysis after dissolution using lithium metaborate/tetraborate fusion with inductively coupled plasma optical emission mass spectrometry (ICP-OES). Averages are reported from extractions run in triplicate and compared to total concentrations from the total digestion of a split sample described above. Samples were sacrificed at each step in the SSE and kept frozen prior for analysis by x-ray diffraction (XRD) and Fe- XANES analysis.

Petrographic Analysis

A split subsample of the <2 mm fraction was air dried under 5% H2/95% N2 and embedded using degassed ultra-clean low-temperature set epoxy (EpoTek 301™). Uniform 30 μm thin sections were cut and ground under an anaerobic environment (Spectrum Petrographics Vancouver, WA). The epoxy-impregnated 30 μm thin sections were bonded to arsenic free quartz slides using cyanoacrylate adhesive (Superglue™). Each thin section was examined with a reflected and cross polarized light microscope. Distinct textural zones and grains of quartz and oxidized v. sulfide grains with and without oxidized rinds were identified in terms of color and morphology (reflected light). Petrographic analysis would have been complicated due to fine grain-size and poorly crystalline nature of the tailings. Electron and synchrotron microprobe (EMPA and u-XRF, respectively) were utilized to further characterize the petrology and elemental associations of the samples. For EMPA, thin sections were carbon coated and analyzed at the Lunar and Planetary Laboratory at the University of Arizona (CAMECA SX100 with WDS), operated at a 15 keV and a beam current of 9.77 nA and a spot size of about 2 μm. Synchrotron x-ray micro fluorescence (μ-XRF) was performed at SSRL. Thin sections further interrogated by micro-focused XRF maps and XAS spectra at the Stanford Synchrotron Radiation Lightsource (SSRL) at 13000 eV and 13050 eV (to differentiate As K-α from Pb L-III) using Si(111) crystal and a Vortex single element detector (SII Nano Technology, Northridge, CA) at beam lines 10-2 and 2-3 with a spot size of 30 μm and 2 μm, respectively.

SSE Fe-XANES Analysis

The SSE-XANES spectra can be used to constrain model fits for complex and heterogeneous natural samples by uncovering phases that would otherwise be overlain and convoluted, making them potentially more difficult to identify. SSE-XANES, as used here without weight adjusted amplitude correction can be used to constrain and identify possible phases, but not the fractional component, used in linear combination fits after targeted phases are dissolved. The method is similar to differential x-ray diffraction can elucidate mineral Bragg reflections lost or gained as a function of reaction in a series of sequential extractions (Dold, 2003; Caraballo et al., 2009). Splits from the IK composite SSE series were examined before and after each SSE by Fe XANES. Examination of the residual revealed isolated phases as well as phases extracted and were used to guide the selection of component models in fits for the pit samples..

Geochemical Modeling

Equilibrium activity diagrams depicting theoretical stability relations among solid phases and aqueous species were computed with the ACT2 program in GWB. Precipitation of the thermodynamically stable phases of hematite, goethite, and magnetite was suppressed in the model to show the metastable phases of ferrihydrite, schwertmannite, and jarosite. Modified database from the LLNL dataset thermo.com.V8.R6+ (Delany and Lundeen, 1990). There are disagreements in the literature on ferrihydrite structure (Waychunas et al., 1993; Zhao et al., 1994; Manceau and Gates, 1997; Janney et al., 2000; Michel et al., 2007), and solubility products (e.g. log K_{sp} = 3.0 to 5.66; Delany and Lundeen, 1990; Majzlan et al., 2004).

Table EA-1: Reference minerals used in XANES linear combination fits, spectra in EA-Figs. 3, 4.

Mineral	**Formula**	**Source**	**Lot/locality**	**Reference**
angelellite	$Fe^{III}_4(AsO_4)_2O_3$	Synthetic		Berdesinski, 1960
anglesite	$PbSO_4$	Aldrich	0731BE	Hayes et al., 2012
ankerite	$Ca(Fe,Mg)(CO_3)_2$	R. Root collection	Pulaski Co., AR	
arsenopyrite	FeAsS	R. Root collection	Ontario, Canada	O'Day et al., 2004a
chlorite	$(Mg, Fe)_5Al(Si_3Al)O_{10}(OH)_8$	Clay Minerals Repository	CCa-2	O'Day et al., 2004b
cinnabar	HgS	Acros Organic	A0231622	
cysteine	$C_3H_7NO_2S$	Fluka	2130945	
elemental sulfur	S	Sigma	11325MI	
ferrihydrite	$Fe_2O_3 \cdot 2FeOOH \cdot 2.6H_2O$	Synthetic		Burleson and Penn, 2006; Gao et al., 2013
goethite	α-$Fe^{III}OOH$	Synthetic		Schwertmann and Cornell, 1991; O'Day et al., 2004b
goslarite	$ZnSO_4 \cdot 7H_2O$	Mallinckrodt	V07616	
greenrust II SO_4	$Fe^{II}_4Fe^{III}_2(OH)_2(SO_4) \bullet 6H_2O$	Synthetic		Drissi, 1995; Root et al., 2009
gypsum	$CaSO_4 \cdot 2H_2O$	Wards Scientific	Alberta, Canada	
hematite	α-Fe_2O_3	Synthetic		Schwertmann and Cornell 1991; O'Day et al., 2004

Mineral	Formula	Source	Lot/locality	Reference
iron (II) sulfate	$FeSO_4$	Fisher Chemicals	040692	
iron (II) sulfide	FeS	Acros Organics	A0244179	
iron (III) sulfate	$Fe_2(SO_4)_3 \bullet 7H_2O$	Aldrich	05517TS	
jarosite	$KFe^{III}_3(SO_4)_2(OH)_6$	Synthetic	na	Driscoll et al., 2005
maghemite	γ-Fe_2O_3	R. Root Collection	Sebkovice Moraiva, Czech Rep.	O'Day et al., 2004b
magnetite	$Fe^{II}Fe_2^{III}O_4$	UCM Collection	San Carlos, AZ	O'Day et al., 2004b
marcasite	FeS_2	Collection of L. Garvie	Lagendorf Hamburg, Germany	O'Day et al., 2004b
melanterite	$Fe(SO_4)\cdot 7H_2O$	Excalibur Mineral		
mercury sulfate	$HgSO_4$	Acros Organics	A0234564	
methionine	$C_5H_{11}NO_2S$	Sigma	058H0123	
orpiment	As_2S_3	Synthetic		Eary 1992; O'Day et al. 2004a
parasymplesite	$Fe^{II}_3(AsO_4)_2 \bullet 8H_2O$	Synthetic	PDF# 00-035-0461	Lin and Puls, 2003
plumbojarosite	$Pb(Fe_3(SO_4)_2(OH)_6)_2$	UA Mineral Museum	5751	Hayes et al., 2009
potassium sulfite	K_2SO_3	Aldrich	04702AH	

Mineral	Formula	Source	Lot/locality	Reference
potassium tetrathionate	$K_2S_4O_6$	Fluka	1157107 51706290	
potassium thiosulfate	$K_2S_2O_3$	Aldrich	11629TD	
pyrite	FeS_2	Wards Scientific	unknown	O'Day et al., 2004b
realgar	α-As_4S_4	UCM collection		O'Day et al., 2004b
schwertmannite	$Fe_8O_8(OH)_6(SO_4)$	Synthetic		Bigham et al., 1990
scorodite	$Fe^{II}AsO_4 \bullet 2H_2O$	UCM collection	Goldhill, Utah	
siderite	$Fe^{II}CO_3$	UCM collection	Chiuahua, Mexico	O'Day et al., 2004b
sodium sulfate	Na_2SO_4	Sigma	117k0004	
sodium sulfite	Na_2SO_3	Sigma	S-8018	
sodium thiosulfate	$Na_2S_2O_3$	J. T. Baker	2946-1	
sphalerite	ZnS	Wards Scientific	Picos de Europa, Spain	
troilite	FeS	UCM collection		
vivianite	$Fe^{II}_3(PO_4)_2 \bullet 8H_2O$	Amethyst Galleries	Kerch, Ukraine	

Table EA-2: Thermodynamic constants and mode conditions for Eh pH diagram

Iron solid	log K
Jarosite $[Fe_3(SO_4)_2(OH)_6]$	9.37 [a]
$3Fe^{3+} + 2SO_4^{2-} + K^+ + 6H_2O \leftrightarrow Fe_3(SO_4)_2(OH)_6 + 6H^+$	
Schwertmannite $[Fe_8O_8(OH)_{4.8}(SO_4)_{1.6}]$	17.4 [b]
$8Fe^{3+} + 12.8H_2O + 1.6SO_4^{2-} \leftrightarrow Fe_8O_8(OH)_{4.8}(SO_4)_{1.6} + 20.8H^+$	
Ferrihydrite $[Fe(OH)_3]$	
$Fe^{3+} + H_2O \leftrightarrow Fe(OH)_3 + 3H^+$	-3.0 [c]
$Fe^{3+} + H_2O \leftrightarrow Fe(OH)_3 + 3H^+$	-5.56 [a]
Pyrite $[FeS_2]$	-24.65 [a,d]
$Fe^{2+} + 0.25SO_4^{2-} + 1.75HS^- + 0.25H^+ \leftrightarrow FeS_2 + H_2O$	

[a] Delaney and Lundeen, 1990; [b] Bigham et al., 1996; [c] Majzlan et al, 2004; [d] Lundeen, 1990

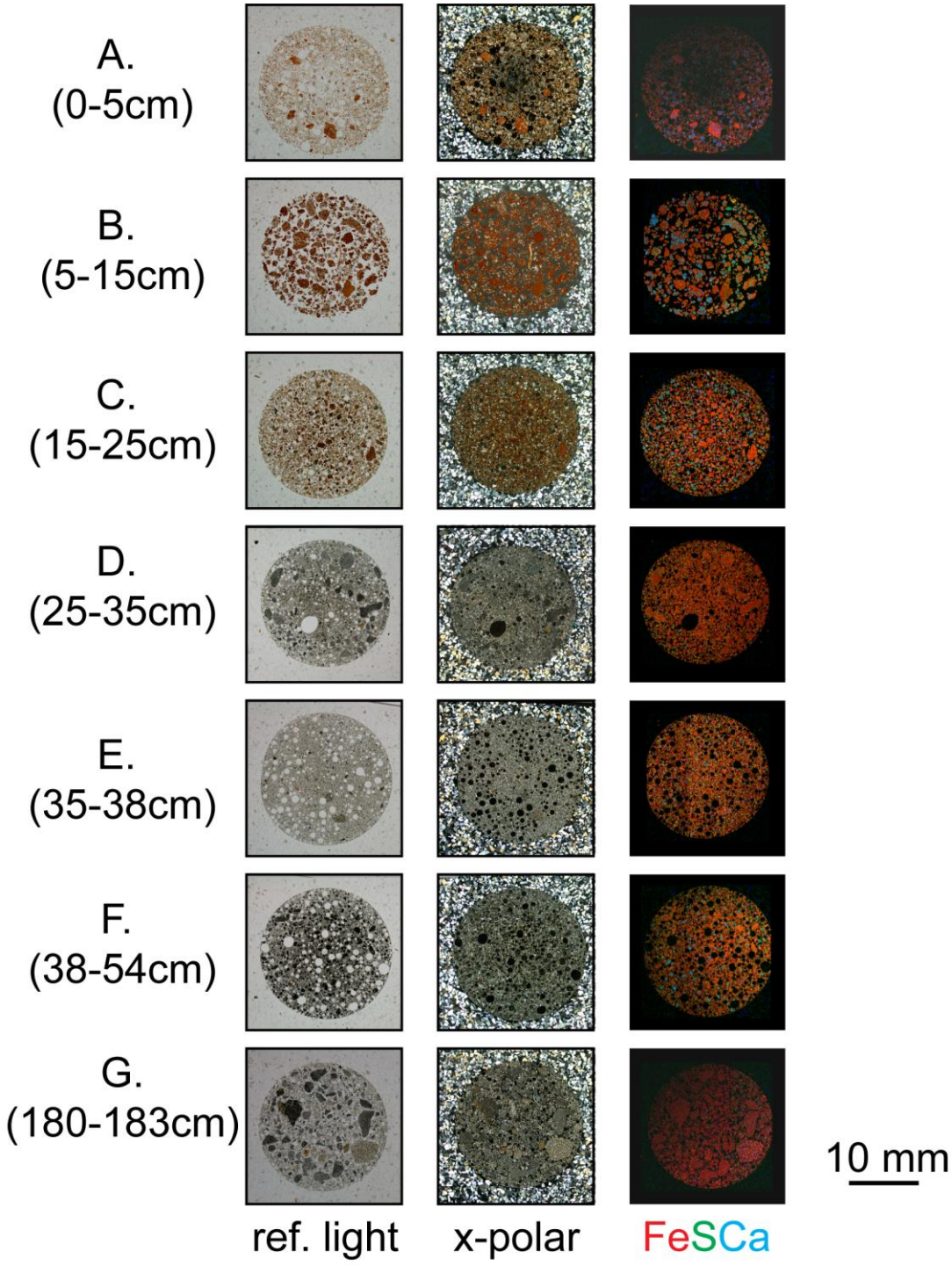

Figure EA-1: Petrographic images of all samples. Images from reflected light, cross polarized light and x-ray fluorescence (13000 & 13050eV) from 30 μm thin sections for each depth (A-G) from the IK mine tailings.

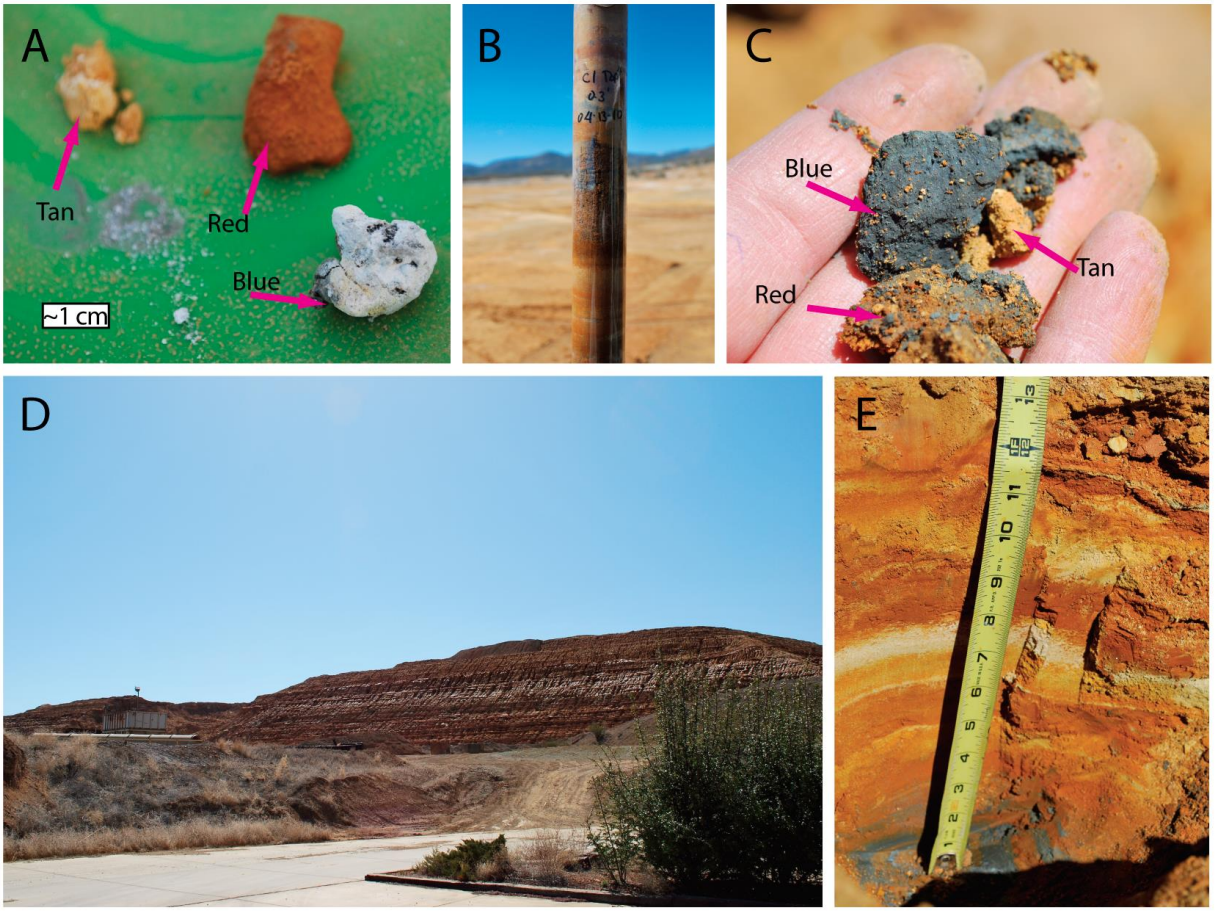

Figure EA-2: Additional information for as-collected samples. Isolated grains were examined based on color and morphology. Panels A-C show the three distinct aggregates observed in the surface tailings, identified as tan, red and blue. Panel D shows the tailings pile observed from the buildings labeled in Fig. 1 with a view to the west toward the pit on top of the pile. Panel E shows the color changes observed in the fresh pit (scale shown in inches).

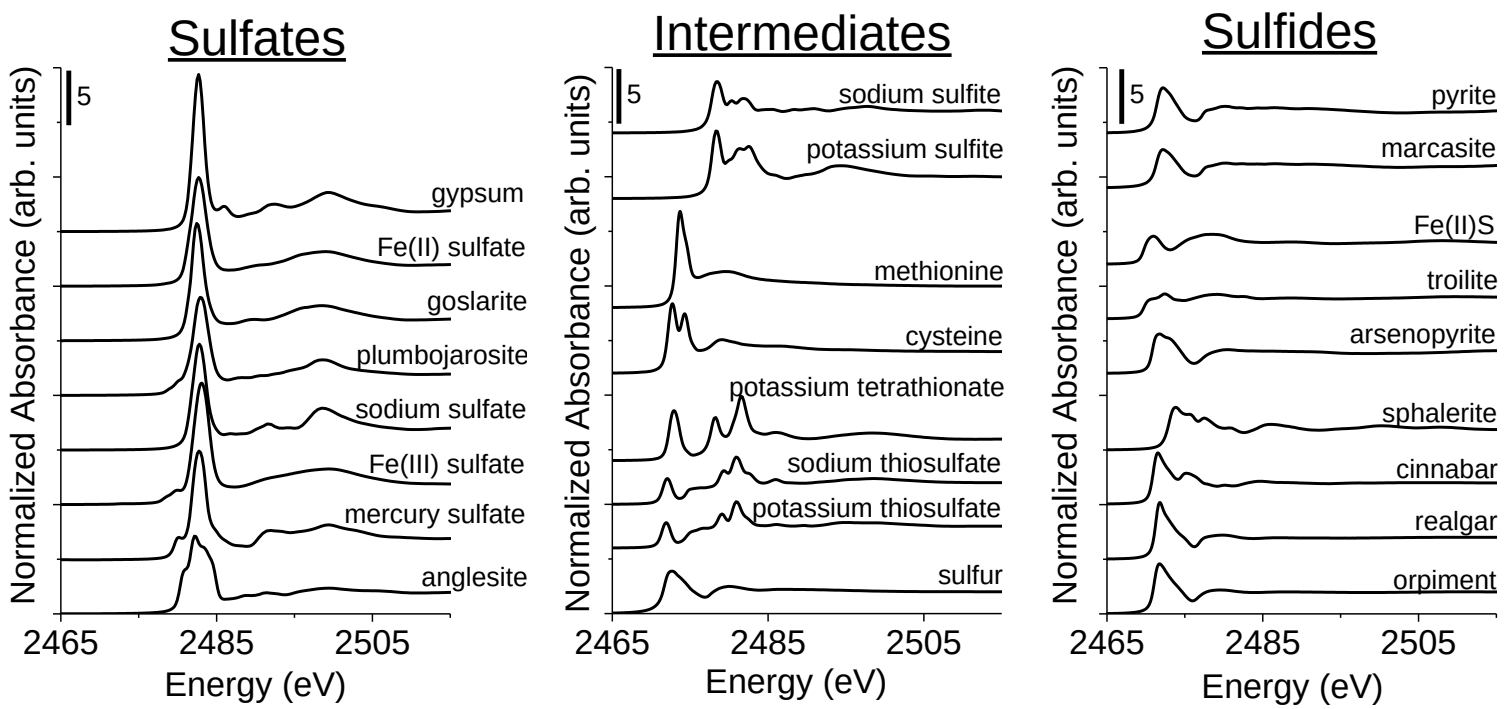

Figure EA-3: Reference minerals used in S XANES linear combination fits

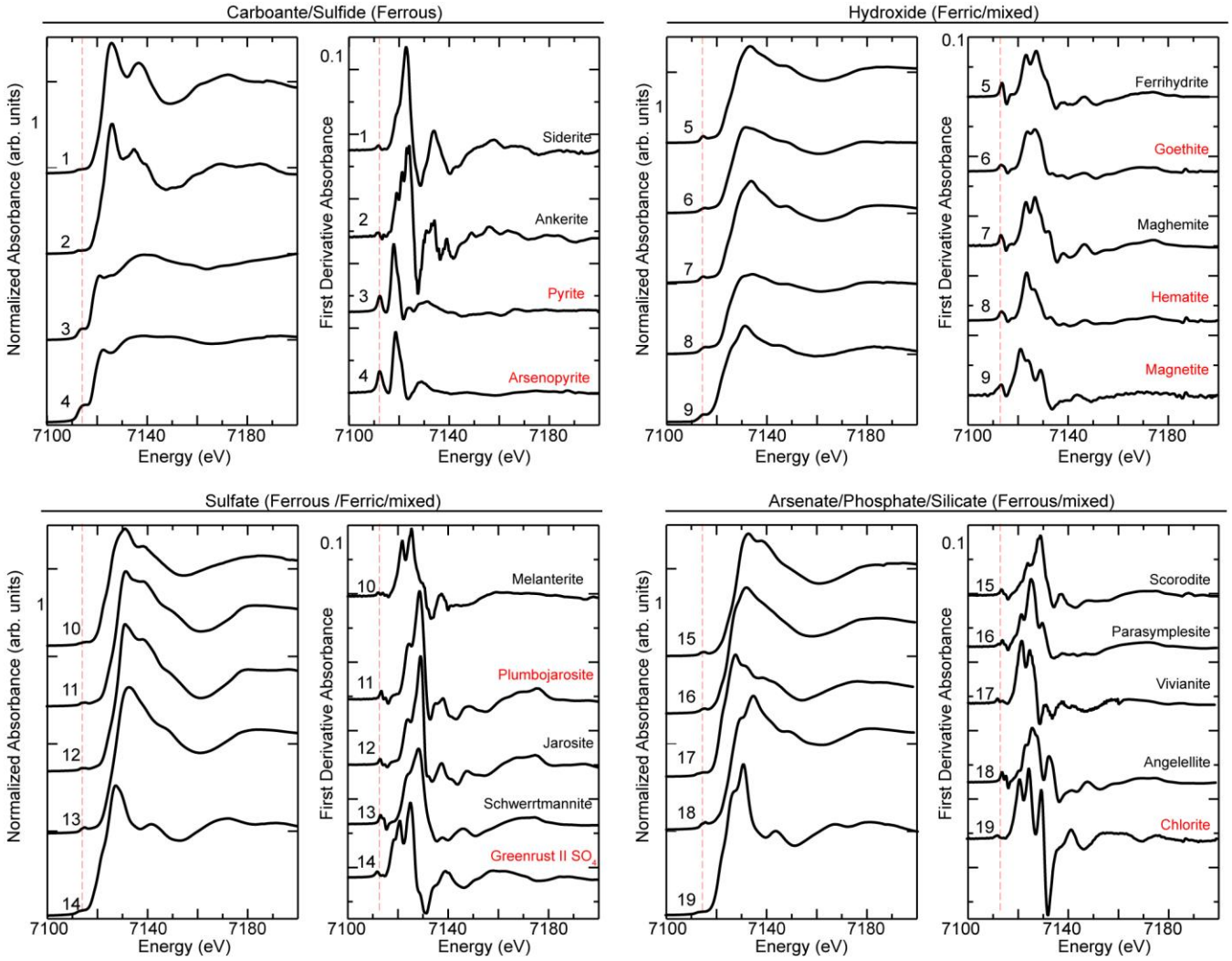

Figure EA-4: Reference minerals used in Fe XANES linear combination fits. Red spectra labels indicate spectra that have been published previously (Hayes et al., 2009; O'Day et al., 2004).

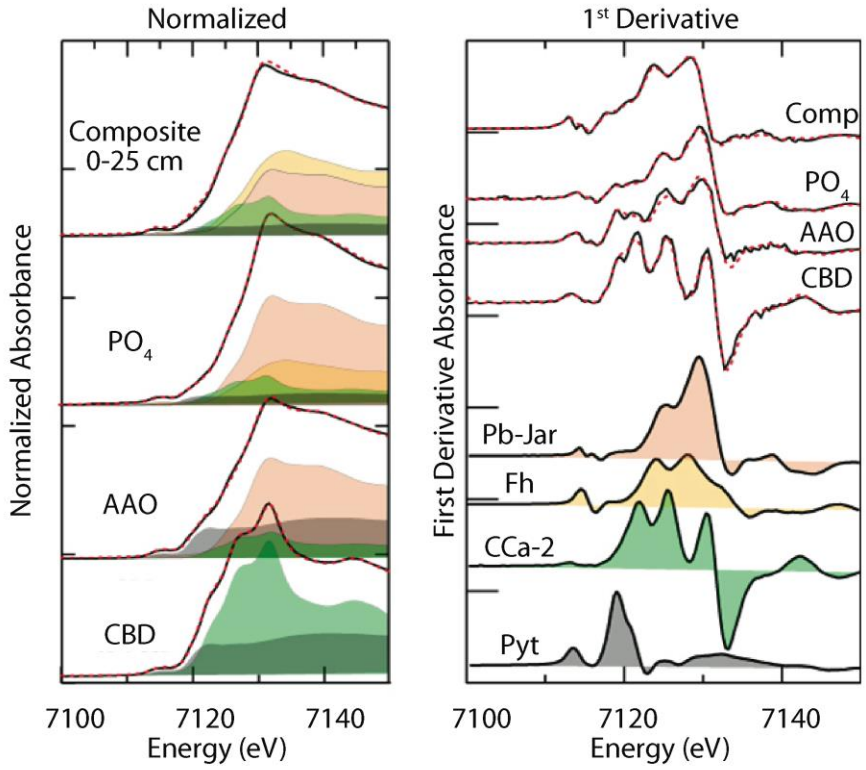

Figure EA-5: First-derivative Fe- XANES fits for SSE samples.

References

Berdesinski, W. W. (1960) Synthesis of angelellite, $(Fe_4(AsO_4)_2)_3$. *Neues Jahrb. Miner. Abh*. **94**, 1203-1208.

Bigham J. M., Schwertmann U., Carlson L., Murad E. (1990) A Poorly Crystallized Oxyhydroxysulfate of Iron Formed by Bacterial Oxidation of Fe(ii) in Acid-Mine Waters. *Geochim. Cosmochim. Acta* **54**, 2743-2758.

Bigham J.M., Schwertmann U, Traina S.J., Winland R.L., Wolf M. (1996) Schwertmannite and the chemical modeling of iron in acid sulfate waters. *Geochim. Cosmochim. Acta* **60**, 2111-2121.

Burleson D.J., Penn R.L. (2006) Two-step growth of goethite from ferrihydrite. *Langmuir* **22**, 402-409.

Caraballo M. A., Rotting T. S., Nieto J. M., Ayora C. (2009) Sequential extraction and DXRD applicability to poorly crystalline Fe- and Al-phase characterization from an acid mine water passive remediation system. *Am. Mineral.* **94**, 1029-1038.

Delany J. M., Lundeen S. R. (1990) The LLNL Thermochemical Database. Report UCRL-21658. Lawrence Livermore National Laboratory

Dold B. (2003) Speciation of the most soluble phases in a sequential extraction procedure adapted for geochemical studies of copper sulfide mine waste. *J. Geochem. Explor.* **80**, 55-68.

Driscoll R. L., Leinz R. W. (2005) Methods for synthesis of some jarosites. *USGS Techniques and Methods 5-D1.*

Drissi S. H., Refait P., Abdelmoula M., and Génin J. M. R. (1995) The preparation and thermodynamic properties of Fe(II)-Fe(III) hydroxide-carbonate (green rust 1); Pourbaix diagram of iron in carbonate-containing aqueous media. *Corros. Sci.* **37**, 2025-2041.

Eary, L. E. (1992) The solubility of amorphous As_2S_3 from 25 to 90 °C. *Geochim. Cosmochim. Acta* **56**, 2267–2280.

Gao X., Root R. A., Farrell J., Ela W., Chorover J. (2013) Effect of silicic acid on arsenate and arsenite retention mechanisms on 6-L ferrihydrite: A spectroscopic and batch adsorption approach. *Appl. Geochem.* **38**, 110-120.

Hayes S. M., White S. A., Thompson T. L., Maier R. M., Chorover J. (2009) Changes in lead and zinc lability during weathering-induced acidification of desert mine tailings: Coupling chemical and micro-scale analyses. *Appl. Geochem.* **24**, 2234-2245.

Hayes S. M., Webb S. M., Bargar J. R., O'Day P. A., Maier R. M., and Chorover, J. (2012) Geochemical Weathering Increases Lead Bioaccessibility in Semi-Arid Mine Tailings. *Env. Sci. Technol.* **46**, 5834-5841.

Janney, D. E., Cowley, J. M., Buseck, P. R. (2000) Transmission electron microscopy of synthetic 2-and 6-line ferrihydrite. *Clay Clay Min.* **48**, 111-119

Lin Z., Puls, R. W. (2003) Potential indicators for the assessment of arsenic natural attenuation in the subsurface. *Adv. Environ. Res.* **7**, 825-834.

Majzlan J, Navrotsky A, Schwertmann U. (2004) Thermodynamics of iron oxides. III - Enthalpies of formation oand stability of ferrihydrite ($Fe(OH)_3$), schwertmannite ($FeO(OH)_{3/4}(SO_4)_{i/8}$), and Fe_2O_3. *Geochim. Cosmochim. Acta* **68**, 1049-1059.

Manceau A., Gates W. P. (1997) Surface structural model for ferrihydrite. *Clay Clay Min.* **45**, 448-460.

Michel F. M., Ehm L., Antao S. M., Lee P. L., Chupas P. J., Liu G., Strongin D. R., Schoonen M. a. A., Phillips B. L., Parise J. B. (2007) The structure of ferrihydrite, a nanocrystalline material. *Science* **316**, 1726-1729.

Neaman A, Mouele F, Trolard F, Bourrie G. (2004) Improved methods for selective dissolution of Mn oxides: applications for studying trace element associations. *Appl. Geochem*. **19**, 973-979.

O'Day P. A., Rivera N., Root R., Carroll S. A. (2004a) X-ray absorption spectroscopic study of Fe reference compounds for the analysis of natural sediments. *Am. Mineral.* **89**, 572-585.

O'Day P. A., Vlassopoulos D., Root R. A., Rivera N. (2004b) The influence of sulfur and iron on dissolved arsenic concentrations in the shallow subsurface under changing redox conditions. *Proc. Natl. Acad. Sci. U.S.A.* **101**, 13703-13708.

Root R. A., Vlassopoulos D., Rivera N. A., Rafferty M. T., Andrews C., O'Day P. A. (2009) Speciation and natural attenuation of arsenic and iron in a tidally influenced shallow aquifer. *Geochim. Cosmochim. Acta* **73**, 5528-5553.

Schwertmann U., Cornell R. M. (2000) *Iron Oxides in the Laboratory: preparation and characterization*. Wiley-VCH Verlag, New York.

Waychunas G. A., Rea B. A., Fuller C. C., Davis J. A. (1993) Surface-Chemistry of Ferrihydrite .1. EXAFS Studies of the Geometry of Coprecipitated and Adsorbed Arsenate. *Geochim Cosmochim Acta* **57**, 2251-2269.

Zhao J. M., Huggins F. E., Feng Z., Huffman G. P. (1994) Ferrihydrite - Surface-structure and its effects on phase transformation. *Clay Clay Min.* **42**, 737-746.